

Bone degradation machinery of osteoclasts: An HIV-1 target that contributes to bone loss

Brigitte Raynaud-Messina^{a,b,c,1}, Lucie Bracq^{d,e,f,2}, Maeva Dupont^{a,b,c,g,2}, Shanti Souriant^{a,b,c,2}, Shariq M. Usmani^{h,i}, Amsha Proag^a, Karine Pingris^{a,b,c}, Vanessa Soldani^j, Christophe Thibault^{k,l}, Florence Capilla^m, Talal Al Saati^m, Isabelle Gennero^{n,o}, Pierre Jurdic^p, Paul Jolicoeur^{q,r,s}, Jean-Luc Davignon^{m,n}, Thorsten R. Mempel^{h,i}, Serge Benichou^{d,e,f}, Isabelle Maridonneau-Parini^{a,b,c,1,3}, and Christel Vérolet^{†a,b,c,1,3}

^aInstitut de Pharmacologie et de Biologie Structurale, Université de Toulouse, CNRS, Université Paul Sabatier, 31400 Toulouse Cedex 4, France; ^bInternational Associated Laboratory, CNRS "Immuno-Metabolism-Macrophages-Tuberculosis/HIV" (1167), 31000 Toulouse, France; ^cInternational Associated Laboratory, CNRS "Immuno-Metabolism-Macrophages-Tuberculosis/HIV" (1167), 1425 Buenos Aires, Argentina; ^dINSERM U1016, Institut Cochin, 75014 Paris, France; ^eCNRS UMR8104, Université Paris Descartes, 75006 Paris, France; ^fInstitut Pasteur Shanghai, Chinese Academy of Sciences, 20000 Shanghai, China; ^gInstitute of Experimental Medicine-Consejo Nacional de Investigaciones Científicas y Técnicas de Argentina, National Academy of Medicine, 1425 Buenos Aires, Argentina; ^hCenter for Immunology and Inflammatory Diseases, Massachusetts General Hospital, Charlestown, MA 02129; ⁱHarvard Medical School, Boston, MA 02115; ^jMultiscale Electron Imaging Platform, 31062 Toulouse, France; ^kLaboratory for Analysis and Architecture of Systems, CNRS, 31400 Toulouse, France; ^lInstitut National des Sciences Appliquées de Toulouse, Université de Toulouse, 31400 Toulouse, France; ^mINSERM, Université Paul Sabatier, École Nationale Vétérinaire de Toulouse, Centre Régional d'Exploration Fonctionnelle et de Ressources Expérimentales, Service d'Histopathologie, 31000 Toulouse Cedex 3, France; ⁿCentre de Physiopathologie de Toulouse-Purpan, INSERM-CNRS UMR 1043, Université Paul Sabatier, 31062 Toulouse, France; ^oInstitut Fédératif de Biologie, Centre Hospitalier Universitaire Toulouse, 31059 Toulouse, France; ^pInstitut de Génomique Fonctionnelle de Lyon, CNRS UMR3444, Université de Lyon, École Normale Supérieure de Lyon, 69007 Lyon, France; ^qDivision of Experimental Medicine, McGill University, Montreal, QC H3G 1A4, Canada; ^rDepartment of Microbiology and Immunology, University of Montreal, Montreal, QC H3T 1J4, Canada; and ^sLaboratory of Molecular Biology, Clinical Research Institute of Montreal, Montreal, QC H2W 1R7, Canada

Edited by Stephen P. Goff, Columbia University Medical Center, New York, NY, and approved January 19, 2018 (received for review July 28, 2017)

Bone deficits are frequent in HIV-1-infected patients. We report here that osteoclasts, the cells specialized in bone resorption, are infected by HIV-1 in vivo in humanized mice and ex vivo in human joint biopsies. In vitro, infection of human osteoclasts occurs at different stages of osteoclastogenesis via cell-free viruses and, more efficiently, by transfer from infected T cells. HIV-1 infection markedly enhances adhesion and osteolytic activity of human osteoclasts by modifying the structure and function of the sealing zone, the osteoclast-specific bone degradation machinery. Indeed, the sealing zone is broader due to F-actin enrichment of its basal units (i.e., the podosomes). The viral protein Nef is involved in all HIV-1-induced effects partly through the activation of Src, a regulator of podosomes and of their assembly as a sealing zone. Supporting these results, Nef-transgenic mice exhibit an increased osteoclast density and bone defects, and osteoclasts derived from these animals display high osteolytic activity. Altogether, our study evidences osteoclasts as host cells for HIV-1 and their pathological contribution to bone disorders induced by this virus, in part via Nef.

osteoclast | HIV-1 infection | bone loss | Nef | podosome

Reduced bone mineral density is a frequent complication of HIV-1-infected patients and often progresses to osteoporosis and high prevalence of fractures. A sixfold increased risk of low bone mineral density is observed in HIV-1⁺ individuals compared with the general population (1). The use of highly active antiretroviral therapy (HAART) has significantly improved the lifespan of patients, revealing these long-term effects of the infection and the persistence of latent proviruses in reservoir cells (2). Multiple factors can contribute to bone loss in infected patients. HAART is one of these factors, especially during the first years of therapy. In addition, there is evidence of bone deficit in nontreated patients, showing that the virus alone alters bone homeostasis (3–6).

Bones undergo continual remodeling, which mainly relies on the sequential actions of bone-resorbing osteoclasts (OC) and bone-forming osteoblasts, under the control of osteocytes (7, 8). In the case of aging or HIV-1 infection, this balance can be disrupted in favor of bone loss. HIV-1-induced bone disorders are associated with an increase of blood biomarkers for bone resorption and minor changes in bone formation-specific markers, suggesting a major contribution of OC in this process (6, 9).

OC are multinucleated cells derived from the monocytic lineage, which have the unique ability to resorb bone matrix. They terminally differentiate by fusion from mononucleated precursors, including blood-circulating monocytes and bone-resident precursors (10). This process is regulated by macrophage colony-stimulating factor (M-CSF) and the key osteoclastogenic cytokine, receptor activator of NF- κ B ligand (RANKL), mainly secreted by osteocytes but also by osteoblasts and activated B and T cells (10, 11). Terminally differentiated OC express high levels of the α v β 3 integrin adhesion receptor and enzymes involved in resorption including cathepsin K, matrix metalloproteinase 9 (MMP9), and tartrate-resistant acidic phosphatase (TRAP). Bone attachment and resorption are mediated

Significance

Bone deficits are frequent complications observed in HIV-1-infected patients. Our study demonstrates that HIV-1 infects osteoclasts, the cells specialized in bone degradation, using different models including HIV-1-infected humanized mice. We decipher the cellular mechanisms by which HIV-1 contributes to enhanced bone degradation in human osteoclasts, showing that the virus modifies the structure and function of the sealing zone, the bone resorption machinery of osteoclasts. We identify the viral protein Nef as the key factor responsible for such effects. As a proof-of-concept, we correlate bone deficit in transgenic Nef-expressing mice with enhanced osteoclast activity. Therefore, our findings provide formal evidence that osteoclasts constitute HIV-1 host target cells, contributing to bone deficits in vivo.

Author contributions: B.R.-M., T.A.S., P. Jurdic, I.M.-P., and C.V. designed research; B.R.-M., L.B., M.D., S.S., S.M.U., A.P., K.P., V.S., C.T., F.C., T.A.S., I.G., J.-L.D., and C.V. performed research; P. Jolicoeur, T.R.M., and S.B. contributed new reagents/analytic tools; B.R.-M., L.B., M.D., S.S., T.A.S., J.-L.D., I.M.-P., and C.V. analyzed data; and B.R.-M., I.M.-P., and C.V. wrote the paper.

The authors declare no conflict of interest.

This article is a PNAS Direct Submission.

Published under the PNAS license.

¹To whom correspondence may be addressed. Email: raynaud@ipbs.fr, maridono@ipbs.fr, or verollet@ipbs.fr.

²L.B., M.D., and S.S. contributed equally to this work.

³I.M.-P. and C.V. contributed equally to this work.

This article contains supporting information online at www.pnas.org/lookup/suppl/doi:10.1073/pnas.1713370115/-DCSupplemental.

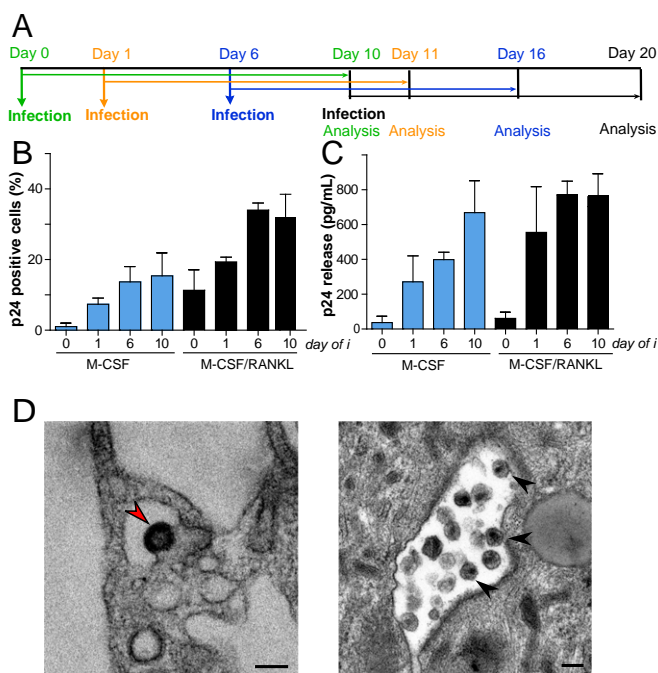


Fig. 2. HIV-1 infects human OC and their precursors in vitro. (A–C) OC are infected by cell-free viruses at different stages of differentiation. (A) Experimental design of infection (ADA strain). (B and C) Kinetics of the percentage of p24⁺ cells (B, determined by IF) and of p24 release in the supernatants (C, determined by ELISA) in cells maintained in M-CSF plus RANKL (OC, black bars) or M-CSF alone (MDM, blue bars) from the same donors are shown. Results are expressed as mean \pm SEM ($n = 3$ donors and 5 donors for day 10). Day of *i*, day of infection. (D) Transmission electron microscopy images of infected OC. Mature OC were infected with HIV-1 and examined 10 d postinfection. Images of a budding virus (Left, red arrowhead) and viruses contained in a cytoplasmic membrane compartment (Right, black arrowheads show mature viruses). (Scale bar, 100 nm.)

10, when cells presented characteristics of mature OC, including high fusion index, high TRAP and MMP9 activities, and bone degradation activity (Fig. S2 A–E). Of note, monocyte-derived macrophages (MDM) from the same donors differentiated with M-CSF (at day 10) only exhibited undetectable or low levels of OC markers, low fusion index, and lacked osteolytic activity (Fig. S2 B–E). Cells were infected in vitro with the HIV-1 R5 ADA strain at day 0, 1, 6, or 10 of differentiation (Fig. 2A). The extent of HIV-1 infection and replication was evaluated at day 10 postinfection by immunofluorescence (IF) analysis of p24 and quantified by measuring the concentration of p24 released in the supernatant. While monocytes (day 0) were poorly able to sustain infection, cells became increasingly permissive to infection along the differentiation process (Fig. 2B and C, black bars); this correlated with the increased expression of the CCR5 entry coreceptor from day 1 (Fig. S2F). Moreover, we observed that virus production was inhibited by pretreatment of OC with the CCR5 antagonist Maraviroc, the reverse-transcriptase inhibitor AZT, the integrase inhibitor Raltegravir, or the protease inhibitor Ritonavir (Fig. S2G), indicating that the p24 signal corresponds to productively infected cells. We noticed that MDM and OC equally sustained infection (Fig. 2B and C) ($\geq 95\%$ donors supported infection, $n = 29$), which is consistent with similar levels of CD4 and CCR5 receptors expressed during differentiation (Fig. S2F) and at day 10 (20). Moreover, the viral particles produced by infected OC or MDM had comparable infectivity, as assessed using the TZM-bl reporter cell line ($27 \pm 5\%$ of p24⁺ TZM-bl for OC-produced particles vs. $26 \pm 7\%$ for MDM, $n = 5$), indicating that both cell types released infectious

virions. Importantly, HIV-1 did not affect OC viability, as cell density was not altered even at day 20 postinfection ($1,580 \pm 276$ nuclei/mm² for noninfected OC vs. $1,560 \pm 352$ for infected OC, $n = 6$ donors, $\geq 3,000$ cells per condition). Finally, we observed virus budding in OC and both mature and immature virus particles accumulating in membrane-delineated intracellular compartments by electron microscopy (Fig. 2D).

Collectively, these results show that HIV-1 infects and replicates in OC and their precursors, without significant cytotoxic effect.

Human OC Are Preferentially Infected by Transmission from Infected T Cells. HIV-1 spreads by infecting target cells either as cell-free particles or more efficiently via cell-to-cell transmission, both in vitro and in vivo (27–30). We thus examined whether mature OC could be infected by contact with infected CD4⁺ T lymphocytes, first using Jurkat T cells infected with the HIV-1 R5-tropic NLAD8-VSVG strain ($>50\%$ of infected T cells, $n = 8$). Briefly, after 6 h of contact with OC, Jurkat cells were washed out (more than 99% of the T cells were eliminated) (Fig. S3A) and OC were harvested either immediately (day 0) or 5 d later (day 5) and stained for intracellular viral p24 by IF (Fig. 3A and B). We observed that 6-h contact (day 0) was sufficient for T cell-to-OC virus transfer with about 15% of p24⁺ OC, while no detectable infection was observed at this time point when OC were cultured with cell-free virions produced by T cells. The difference was maintained at day 5. At this time point, the high rate of infected OC could result from the initial infection by T cell-to-OC transmission and from enhanced OC cell fusion. Noticeably, virus transfer via infected T cells led to a productive infection of OC as shown by the amount of p24 detected in the supernatant at day 5 (Fig. 3C), which is higher than in the case of infection with cell-free virions. Finally, we confirmed the efficient virus transfer from infected T cells leading to productive infection of

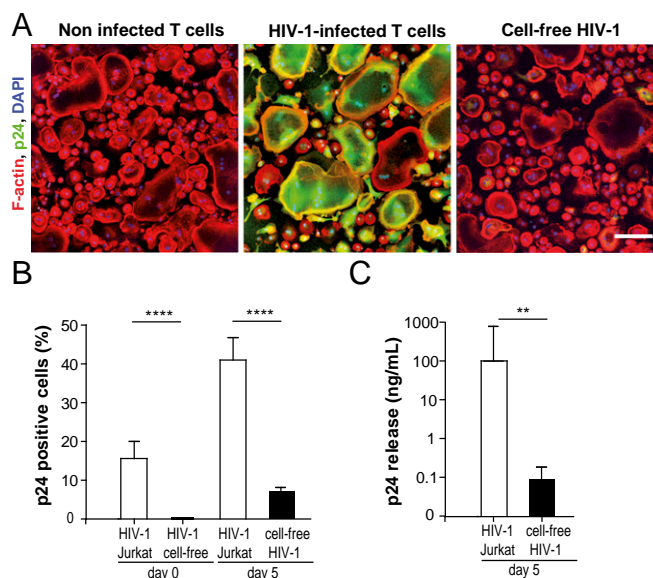


Fig. 3. HIV-1 is transmitted from infected T lymphocytes to OC. (A–C) OC have been in contact for 6 h with noninfected Jurkat T lymphocytes (Left), with HIV-1-infected T lymphocytes (Center), or with cell-free viral particles produced by T cells during 6 h (Right); they were washed, then harvested immediately (day 0) or 5 d later (day 5). (A) Representative mosaic of 3×3 confocal fields of original magnification 20 \times , after staining for p24 (green), F-actin (phalloidin-Texas red, red), and nuclei (DAPI, blue) at day 5. (Scale bar, 50 μ m.) (B and C) Quantifications (mean \pm SD, $n = 8$ donors) of the percentage of p24⁺ cells evaluated by IF (B) immediately (day 0) or 5 d (day 5) postinfection and of p24 release in the supernatants determined by ELISA after 5 d (day 5) (C). ** $P \leq 0.01$; **** $P \leq 0.0001$.

OC by using autologous infected T lymphocytes as virus donor cells (Fig. S3 B and C).

These results show that OC are not only infected by cell-to-cell transfer via infected T cells, but it is also more efficient than infection by cell-free virions.

HIV-1 Infection Enhances OC Precursor Migration and OC Bone Resorption Activity. In HIV-1 transgenic rats, severe bone loss has been correlated to an increase in the number and size of OC (18). This increase could reflect an enhanced recruitment of OC precursors or a stimulated OC differentiation. We tested both hypotheses. It is known that migration of OC precursors from blood to bones requires proteases *in vivo* (31), and that defects in the 3D protease-dependent mesenchymal migration of these cells *in vitro* correlates with lower recruitment of OC to bones (16). For these reasons, we assessed whether HIV-1 infection alters OC precursor mesenchymal migration (32, 33). Human OC precursors were infected at day 1 of differentiation, seeded at day 2 on Matrigel, and migration was measured 48 h later (Fig. 4). Of note, OC precursors inside Matrigel exhibited the characteristic elongated shape of the mesenchymal migration (32). The percentage of migrating cells and the distance covered by the cells were both significantly increased upon HIV-1 infection.

Next, to test whether HIV-1 infection affects OC differentiation, we examined the consequences of infection on the extent of OC fusion and bone resorption activity. HIV-1 infection significantly enhanced cell fusion, as measured by the fusion index and the area covered by infected versus noninfected OC (Fig. 5A), the percentage of TRAP⁺ multinucleated cells, and the number of nuclei per multinucleated cell (Fig. S4 A and B). When cells were treated with Maraviroc before infection, the fusion index was reduced to a similar level to controls (Fig. S4C). Moreover, to explore the effects of OC infection on bone resorption activity, we characterized the morphology of the resorption lacunae. The total bone resorption area increased upon HIV-1 infection (Fig. 5 B–D) and resorption pits displayed profound morphological modifications (Fig. 5 B–F). Infected OC generated resorption pits that appeared deeper ($28 \pm 1.2 \mu\text{m}$ vs. $17 \pm 0.7 \mu\text{m}$ for controls, $***P < 0.0001$) (Fig. 5C) and less elongated (Fig. 5E) than those of noninfected OC, which form resorption trails reminiscent of “inchworm-like migration” (34). These modifications correlated with a significant up-regulation of the bone

volume resorbed per pit in the HIV-1 infection context (Fig. 5F). Furthermore, we also found a significant increase in the concentration of the C-terminal telopeptide of type 1 collagen (CTX) released in the supernatants and used as an additional marker of bone resorption (Fig. 5G).

Osteolytic activity is mediated by acidic dissolution of the minerals and enzymatic digestion of the organic components (35). HIV-1 infection enhanced these two activities, as evidenced by the increase in the capacity of OC to dissolve minerals (Fig. 5H) and release TRAP (Fig. 5I). No variation in protein expression and activity was noticed regarding secreted cathepsin K and MMP9 (Fig. 5 J and K).

Finally, we examined OC attachment/detachment, a critical factor for bone degradation (12), given that OC resorption partly proceeds through a succession of migratory phases alternating with bone resorption stationary phases (12, 36). When infected, OC were more resistant to detachment induced by Accutase treatment than noninfected counterparts (Fig. 5L). This increased adhesion likely slows down OC motility on bone, which should contribute to the modified morphology of resorption lacunae and to the higher bone degradation activity.

All in all, these results indicate that HIV-1 infection enhances the 3D migration of OC precursors, which may favor recruitment of OC to bones, as well as the adhesion and bone resorption activity of mature OC.

HIV-1 Infection Alters the Architecture of the SZ and Activates Src Kinase. Because the SZ has been related to adhesion and bone degradation capacities of OC (11, 37), we characterized the architecture of this structure in infected OC. We observed that in OC seeded on bones, the number of cells harboring SZ was increased (Fig. 6 A and B). This effect was not duplicated by infection with *Mycobacterium tuberculosis*, *Francisella novicida*, or *Salmonella typhimurium* (infection rates $\geq 50\%$ for each bacteria, percentage of cells harboring SZ: 18 ± 9 for *M. tuberculosis*, 22 ± 6 for *F. novicida*, 25 ± 4 for *S. typhimurium* vs. 25 ± 10 in noninfected OC, mean \pm SD, $n = 4$), suggesting that this parameter was not generally influenced by OC infection. In addition, the size of the SZ was increased (Fig. 6 A and C), delineating an area corresponding to $25 \pm 1\%$ of the cell surface of infected OC vs. $18 \pm 2\%$ in control cells (Fig. 6D). We also noticed that the fluorescence intensity of F-actin was higher in the SZ of infected cells (Fig. 6 A and E) and the F-actin core of podosomes, the basal element of the SZ, was larger (Fig. 6 F and G). The tyrosine kinase Src plays a key role in bone homeostasis by controlling the formation and stability of the SZ and the rate of actin turnover within OC podosomes (14, 16, 38). Consequently, OC from *Src*^{-/-} mice do not assemble functional SZ and the mice exhibit a strong osteopetrotic phenotype (15). Interestingly, we showed that in the context of HIV-1-infected OC, the activity of Src kinase family was enhanced as measured by phosphorylation of the regulatory tyrosine (Fig. 6H).

These results show that the increase in bone adhesion and resorption observed in infected OC is associated with larger and more numerous SZ as well as higher Src kinase activity.

The Viral Factor Nef Is Involved in HIV-1-Induced Effects on OC Both *In Vitro* and *In Vivo*. To better understand the viral mechanisms involved in HIV-1-induced effects in OC, we focused on the viral accessory factor Nef because it is known, among other functions, to modulate F-actin organization and to stimulate both the kinase activity of Src (39–44) and cell fusion (45). To this end, we used *wt* HIV-1 and *nef*-deleted HIV-1 (δnef /HIV-1) ADA strains that present the same level of infectivity in macrophages (33, 45–47) and in OC (Fig. S5A). Importantly, the viral particles produced by OC infected with the *wt* or mutant strains showed the same level of infectivity ($26 \pm 7\%$ of p24⁺ TZM-bl cells for the *wt* strain vs. $22 \pm 5\%$ for δnef /HIV-1, $n = 4$). As shown in Fig. 7A,

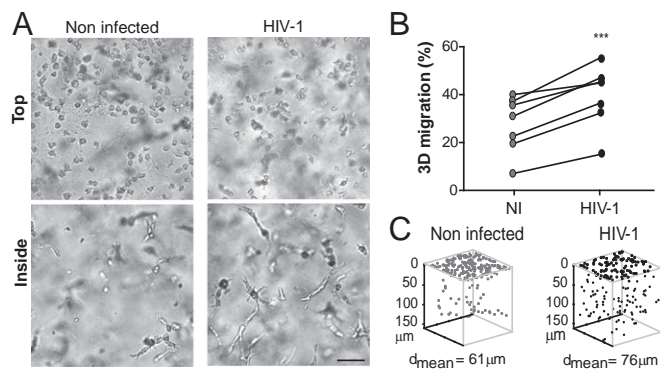


Fig. 4. HIV-1 enhances 3D migration of OC precursors in Matrigel. OC precursors were infected or not at day 1, seeded at day 2 on thick layers of Matrigel polymerized in transwell chambers, and migration was measured 48 h later. (A) Representative brightfield images of live cells either at the surface (top) or within the matrix (inside), taken after 48 h of migration using an inverted video microscope. (Scale bar, 50 μm .) (B) The percentage of migrating cells was measured (mean \pm SEM, $n = 7$ donors) (NI, noninfected). $***P \leq 0.001$. (C) Three-dimensional positions of OC precursors in the matrix and mean distance of migration (d_{mean}) from a representative experiment of seven are shown using the TopCat software.

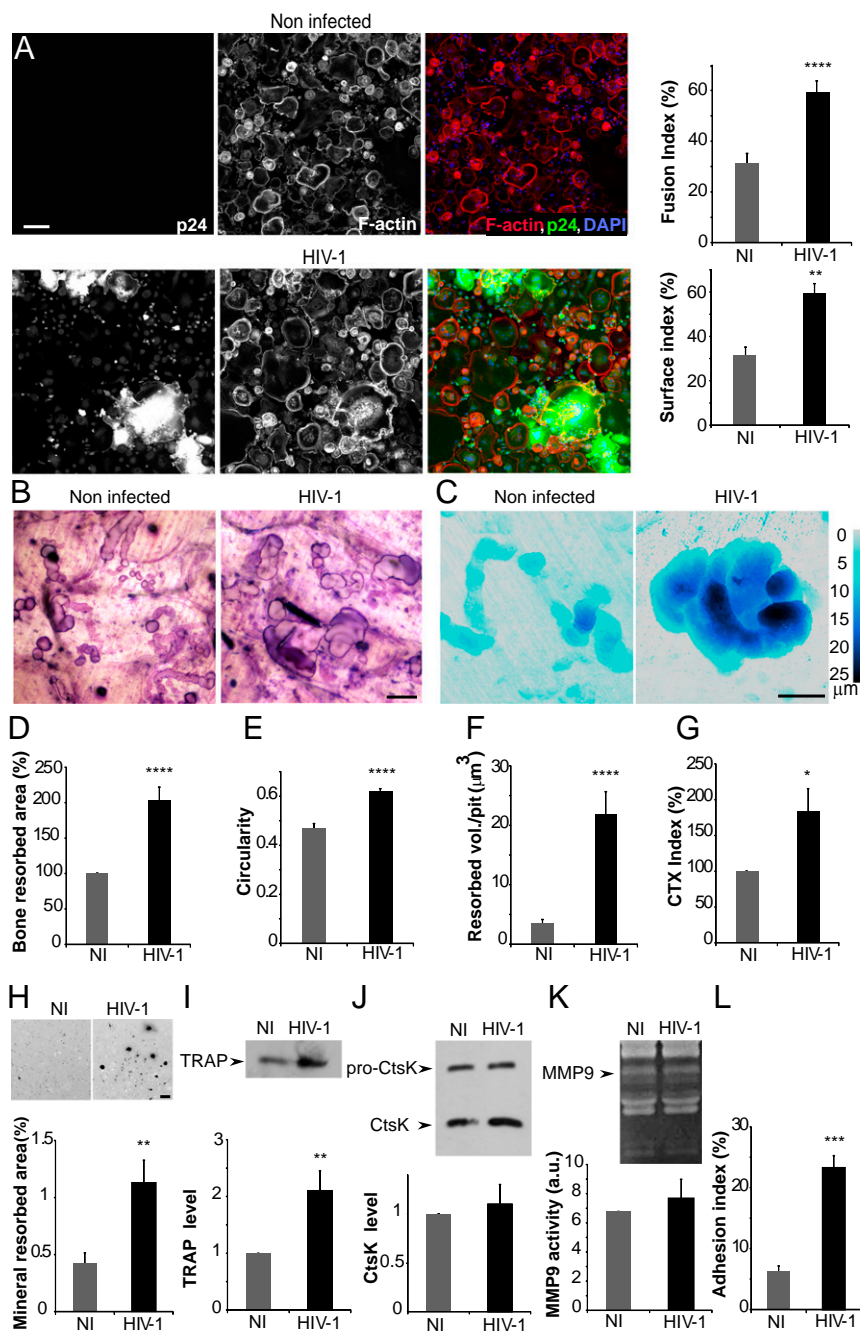


Fig. 5. HIV-1 enhances OC fusion, osteolytic activity, and adhesion of OC. (A) HIV-1 triggers OC fusion. Ten days postinfection, cells were stained for p24 (green), F-actin (red), and nuclei (blue). Images from a mosaic of 4×4 confocal fields of original magnification 20 \times . (Scale bar, 150 μ m.) The cell fusion index (nuclei number in multinucleated cells/total nuclei number) and the surface percentage covered by multinucleated cells (surface index) were measured for $>3,000$ cells in each condition, $n = 6$ donors. Results are expressed as mean \pm SEM. (B–G) HIV-1 infection increases the bone resorption activity of OC. Day 10-noninfected and HIV-1-infected OC were seeded on cortical bone slides for 48 h. Then, OC were removed, the supernatants collected, and the bone slices stained with Toluidine blue to visualize resorption pits in purple. Data were obtained from six donors. (B) Representative brightfield images of bone-resorption pits (purple). (Scale bar, 20 μ m.) (C) Representative confocal images of pits. Color codes for the depth of resorption pits (color scale bar). (Scale bar, 20 μ m.) Quantification of the percentage of degradation area (D) and circularity (E) from brightfield images and resorbed volume (F) from confocal images are shown. In D, the degradation area of noninfected OC, normalized to 100%, corresponded to 9% of the total area. (G) The concentration of CTX in the supernatant was measured by ELISA and normalized to 100% for noninfected cells (mean CTX concentration = 1,790 pg/mL), $n = 6$ donors. (H–K) Effects of infection on mineral dissolution and extracellular osteolytic enzymes. (H) Day 10-noninfected and HIV-1-infected OC were seeded on crystalline inorganic calcium phosphate-coated multiwells. The cells were removed and the wells stained to reveal demineralized area (black). (Scale bar, 50 μ m.) Graph shows the area covered by mineral dissolution pits from 10 fields per condition and per donor, $n = 3$ donors. (I–K) The supernatants of noninfected and HIV-1-infected OC seeded on glass were collected at day 10. TRAP and CtsK expression levels (Western blot, I and J) and MMP9 activity (zymography analysis, K) were quantified. Protein loading has been controlled by Coomassie blue staining, $n = 4$ donors. (L) HIV-1 infection increases OC adhesive properties. Noninfected and HIV-1-infected OC were removed at day 10 with Accutase for 10 min and the percentage of remaining adherent cells quantified by counting nuclei (adhesion index). Graph represents average of five fields per condition from $n = 3$ donors (NI, noninfected). * $P \leq 0.05$; ** $P \leq 0.01$; *** $P \leq 0.001$; **** $P \leq 0.0001$.

the 3D mesenchymal migration of OC precursors infected with δ nefHIV-1 was similar to noninfected cells. In mature OC, Src kinase phosphorylation, bone resorption activity, percentage of cells with SZ, fusion index, and SZ area were reduced in δ nefHIV-1-infected OC in comparison with cells infected with the *wt* virus (Fig. 7 B–F).

Next, we considered performing ectopic expression of Nef-GFP in OC, but we encountered a technical limitation; only 5% of Nef-expressing cells were obtained, precluding a rigorous quantification of SZ size and bone resorption activity. Nonetheless, when the transfected cells were plated on glass, we observed a fraction of Nef-GFP localized at the SZ on bones and that podosomes occupied a larger area than those of control cells (Fig. 7 G and H), thus mimicking the results obtained with OC infected with the *wt* virus (Fig. 6 F and G).

Next, we took advantage of transgenic (Tg) mice expressing Nef under the regulatory sequence of the human CD4C gene to overcome the transfection difficulty of human OC. The CD4C regulatory element drives Nef expression in CD4⁺ T cells, macrophages, and dendritic cells (48, 49), and also in OC (Fig. S5B). In fact, in the absence of any available Nef antibody for IHC, we used CD4C/HIV-1^{GFP} Tg mice. We verified that the GFP was expressed in all OC, indicating that CD4C drives the expression of ectopic genes in OC (Fig. S5B). To characterize the effects of Nef expression in OC, OC precursors were isolated from bone marrow of Nef-Tg and non-Tg mice and differentiated ex vivo. While the fusion of OC from Nef-Tg mice was not modified compared with OC derived from control mice (Fig. 8A), the bone resorption (Fig. 8B) and the width of F-actin staining in the SZ were enhanced (Fig. 8 C and D), indicating that Nef expression is sufficient to increase the osteolytic activity of OC.

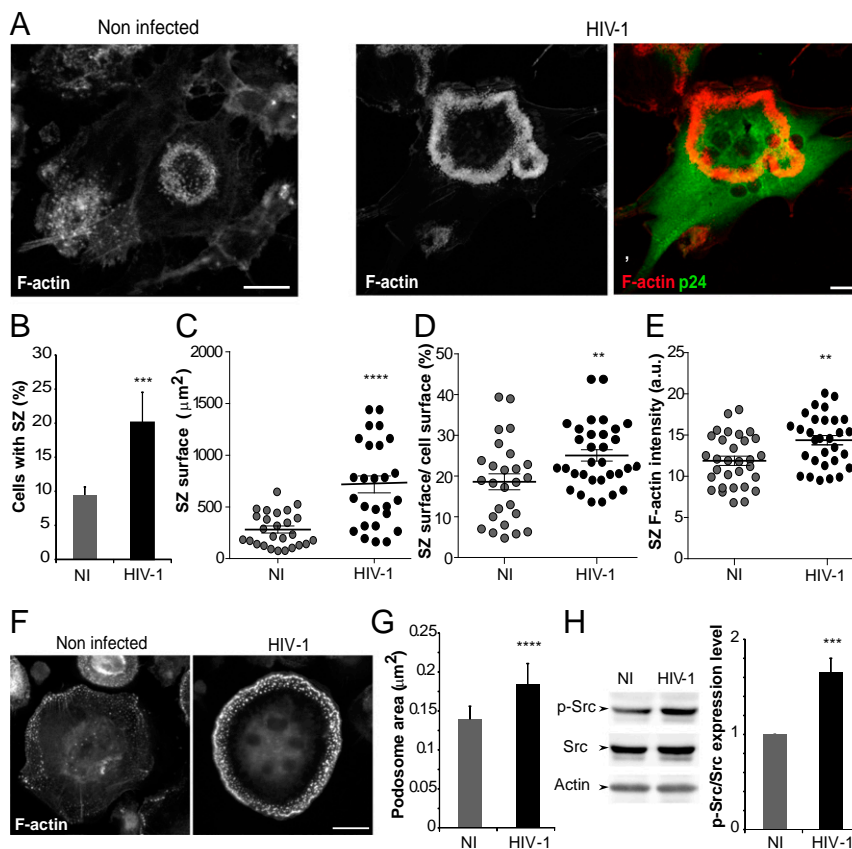


Fig. 6. HIV-1 modifies the organization of the SZ and induces Src-kinase activation in human OC. (A–E) HIV-1 infection increases the size and F-actin intensity of the SZ. (A) Confocal images of noninfected or HIV-1-infected OC seeded on bone slides. Cells were stained for p24 (green) and F-actin (red). (Scale bar, 10 μm.) (B) Quantification of the percentage of cells forming SZ ($n = 4$ donors, 300 cells per donor). (C–E) Vertical scatter plots showing for each SZ, the surface (C), the percentage of the cell surface occupied by SZ (D), and the F-actin intensity (E) ($n = 3$ donors, >25 SZ). Graphs show individual SZ values and the mean \pm SEM. (F and G) HIV-1 infection increases the size of individual podosomes. OC seeded on glass were infected with HIV-1 and stained for F-actin. (F) IF images. (Scale bar, 10 μm.) (G) Automated quantification of the F-actin fluorescence area of individual podosomes. Mean \pm SEM, $n = 3$ donors (>2,000 podosomes, 10 cells per donor). (H) HIV-1 infection induces Src-kinase activation. Whole-cell lysates were subjected to Western blotting using antibodies against the phospho-Tyr416 of Src kinases, Src and Actin. A representative blot and quantification of the phospho-Tyr416 kinase ratio over total Src are shown. Results are expressed as mean \pm SEM, $n = 6$ donors (NI, noninfected). ** $P \leq 0.01$; *** $P \leq 0.001$, **** $P \leq 0.0001$.

Finally, we addressed the role of Nef on bone remodeling in vivo. Nef-Tg mice exhibited bone defects as evidenced by abnormal bone fragility during dissection and by an overall decrease in bone density (Fig. S5C). In tibia growth plates of 7-wk-old female mice, we observed a decrease of the bone area (trabecular surface) in Nef-Tg mice compared with non-Tg mice (Fig. 8 E and F, gray), and a disorganized hypertrophic chondrocyte zone (Fig. 8E, delineated by the red line), which appeared thinner and irregular. Moreover, a marked increase in TRAP⁺ signal was noticed (Fig. 8 E and F, purple), indicating that OC were larger and more numerous in Nef-Tg mice compared with control littermates.

Altogether, these results support that the viral protein Nef is sufficient to increase the osteolytic activity of OC and, thereby, potentially contribute to bone loss in vivo.

Discussion

Bone defects resulting from HIV-1 infection have long been described, but the causes remain poorly investigated (1). We report that HIV-1 infects OC in vivo, ex vivo, and in vitro. In infected OC, the structure and function of the SZ are modified, affecting bone attachment and resorption. The viral protein Nef is instrumental in these processes. Hence, OC are cell targets for HIV-1, which is, to our knowledge, the only pathogen able to manipulate the SZ.

Using HIV-1-infected BLT-humanized mice, we obtained evidence of the presence of infected OC in bones. Infected OC appear as a rare event, either due to the moderated viremia (we worked shortly after infection) and low sensitivity of the IHC detection, or to the fact that infected OC are poorly detected in tissues similarly to infected macrophages (22, 50–54). OC can also be infected ex vivo in fresh human synovial explants. Importantly, OC infection in vivo and ex vivo was detected by IHC of the viral p24, which is suggestive of viral replication. In vitro, electron microscopy images of infected OC revealed that the virus particles bud and accumulate in intracellular compartments, suggestive of the virus-containing compartments described in macrophages (55–57). The virus production by OC was quantitatively similar to that of macrophages, a well-known HIV-1 host cell (21, 22, 58). Infection of OC occurred at different time points along the differentiation process, starting at day 1 in OC precursors and correlating with CCR5 expression. This suggests that circulating OC precursors, which encounter the virus in blood, could become infected and migrate to bones, where they terminally differentiate (59, 60) (Fig. 9). Whether mature OC can be infected directly in bones is difficult to explore. Up to now, the presence of HIV-1 in bones has not been documented. As recently shown for macrophages (61), direct contact of OC with infected Jurkat or primary CD4⁺ T lymphocytes leads to virus transfer and productive infection of OC,

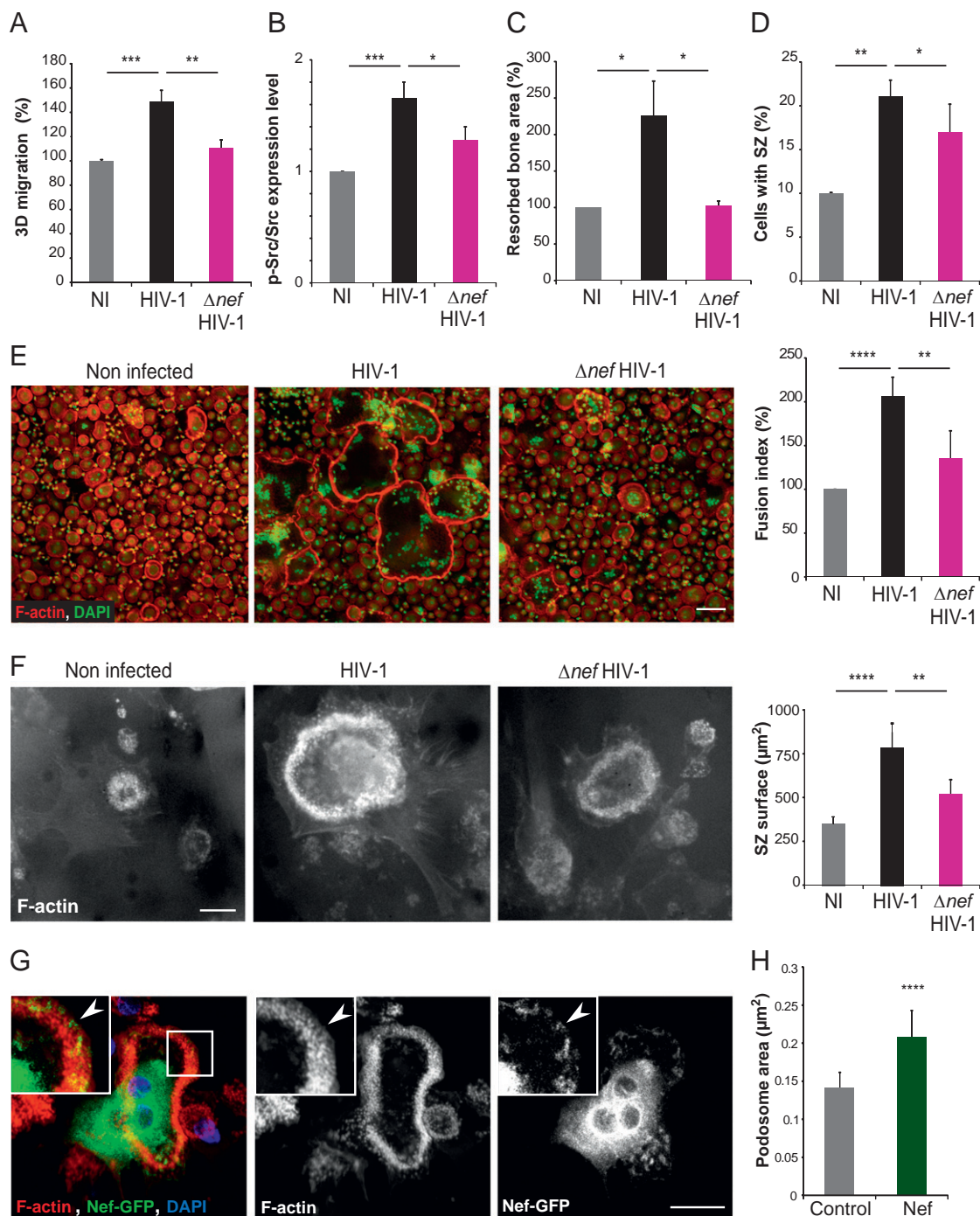


Fig. 7. HIV-1 effects on differentiation and function of OC involve the viral protein Nef. (A–F) Nef is necessary for HIV-1-induced effects in OC. Human OC precursors (A) or mature OC (B–F) were infected with *wt* HIV-1 or with delta *nef*HIV-1 (NI, noninfected). (A) Percentage of migrating OC precursors after 48 h measured as in Fig. 4, $n = 4$ donors. (B) Quantification of Western blot analyses on whole-cell lysates using antibodies against the phospho-Tyr416 of Src kinases, Src and Actin as in Fig. 6H. Results are expressed as mean \pm SEM, $n = 6$ donors. Quantification of (C) resorbed bone area ($n = 4$), (D) the percentage of cells forming SZ ($n = 4$ donors, 300 cells per donor), (E) the fusion index ($>3,000$ cells per condition, $n = 6$ donors) illustrated by mosaics of 4×4 confocal fields (F-actin in red and nuclei in green), (F) the SZ surface in OC seeded on bones and stained for F-actin (phalloidin), ($n = 3$ donors, >25 SZ). (Scale bars, 150 μm in E, 10 μm in F.) Results are expressed as mean \pm SEM. (G and H) Expression of Nef-GFP in OC. OC were transfected with Nef_{SF2}-GFP or GFP (control) and stained for F-actin (phalloidin, red) and nuclei (blue). (G) A fraction of Nef localizes at the SZ. Confocal images of OC expressing Nef_{SF2}-GFP. Arrowheads show colocalization of Nef-GFP with F-actin at the SZ. (Scale bar, 10 μm , Insets, 2 \times zoom.) (H) Nef expression increases the size of individual podosomes. Automated quantification of the F-actin fluorescence area of individual podosomes. Mean \pm SEM, $n = 4$ donors ($>2,000$ podosomes from over five cells per donor). * $P \leq 0.05$; ** $P \leq 0.01$; *** $P \leq 0.001$, **** $P \leq 0.0001$.

which is clearly more efficient than infection by cell-free viruses. This is likely to be the physio-pathological route to infect OC in situ, which would be consistent with data showing that cell-to-cell

infection is critical for efficient viral spread in vitro and in vivo (25, 29, 61–69). Altogether, these results show that OC are host cells for HIV-1.

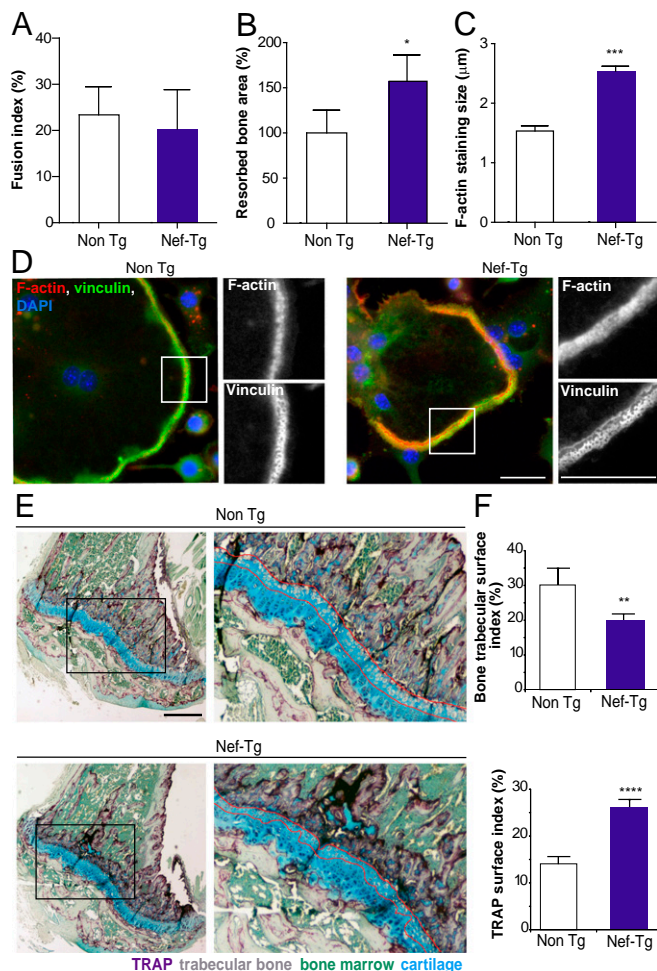


Fig. 8. In Nef-Tg mice, the osteolytic activity of OC and bone defects are enhanced. (A–D) OC differentiated ex vivo from Tg-mice are more osteolytic. OC were differentiated from bone marrow precursors isolated from Nef-Tg and non Tg mice and the fusion index (A), the bone resorption area (B), and the F-actin belt thickness (C) were quantified (50 SZ per condition, $n = 3$ mice per genotype). (D) Representative images of belt structures of OC from non Tg and Nef-Tg mice stained for F-actin (red), vinculin (green) and DAPI (blue). Enlarged frames, 2 \times zoom. (Scale bars, 10 μ m.) (E and F) Nef-Tg mice exhibit bone defects. (E) Representative histological sections of tibia from 7-wk-old mice stained for TRAP to visualize OC (purple), and counterstained with Methyl green and Alcian blue: the bone tissue appears in gray, nuclei in green (corresponding to the nuclei of bone marrow cells), and cartilage in blue. (Scale bar, 200 μ m.) Enlarged frames: $\times 4$ zoom. (F) Quantification of the surface occupied by trabecular bone and surface occupied by TRAP-positive signal in three separate histological sections per mouse ($n = 3$ mice per genotype) are shown. * $P \leq 0.05$; ** $P \leq 0.01$; *** $P \leq 0.001$, **** $P \leq 0.0001$.

Regarding the consequence of HIV-1 infection on OC function, along with this study, there is another report describing that the bone resorption activity of infected OC is exacerbated (20). Herein, we revealed potential mechanisms involved in enhanced bone resorption that concern the structure and function of the SZ, the cell structure instrumental for bone resorption. SZ are larger in HIV-1-infected OC and, consequently, they can degrade larger bone areas. This is in line with the formation of giant OC, which contain twice as more nuclei when they are infected. This exacerbated bone degradation by HIV-1-infected OC also resulted from an increased demineralization process combined with an enhanced secretion of TRAP. The SZ is made of densely connected podosomes, F-actin-rich cell structures involved in cell adhesion, mechanosensing, and cell migration

(70). SZ assembly and patterning are under the control of Src (14, 38). Interestingly, we report that the Src kinase activity was activated in infected OC and that podosomes were enlarged, as visualized by an increase of F-actin staining. In human macrophages, modifications of the F-actin content in individual podosomes have been correlated with fluctuations of protrusion forces exerted onto the extracellular matrix by these cell structures (71). In OC, these modified podosomes may promote more efficient sealing to bone surface. Indeed, we observed stronger adhesion for HIV-1-infected OC compared with noninfected OC. Because the SZ is a barrier that limits the diffusion of acidic and proteolytic molecules released in the resorption lacunae (11–14), increased adhesion would likely enhance the efficiency of containment and favor bone resorption (72). From these results, we propose that modification of several parameters of the SZ (i.e., increased size, adhesion, and degradative activity) contribute to the enhanced osteolytic activity and to the modifications of the topography of resorption pits on infection (12, 36, 73). Pharmacological destabilization of the SZ would reduce the impact of HIV-1 on bone degradation. Several ongoing therapeutic strategies, including the inhibition of the SZ component DOCK5 or cathepsin K activity, are being developed to reduce osteoporotic syndromes while preserving OC viability and differentiation, and thus bone homeostasis (17, 74, 75). We also noticed that OC precursors displayed an enhanced ability to migrate when infected with HIV-1. Interestingly, the efficiency of OC precursor migration has been correlated to OC density in bones (10, 16). Therefore, in addition to enhanced bone resorption activity of infected OC, increased migration of OC precursors should favor OC recruitment to bones, as depicted in Fig. 9, contributing to bone disorders in infected patients.

Nef is a crucial determinant of viral pathogenesis and disease progression. It is known to physically interact with several host proteins to control their activity at the benefit of the virus. Namely, it regulates intracellular protein trafficking (76), actin cytoskeleton (41), cell–cell fusion (45), cell migration (33, 42, 77, 78), and the kinase activity of several members of the Src family (40). In infected OC, all these effects could contribute to the enhanced bone resorption activity that is observed in the present study. In vitro experiments show that Nef, in part located at the SZ, was necessary for all of the HIV-induced effects. The role of Nef was also revealed in vivo in CD4C-Nef-Tg mice that exhibit reduced bone density and an increase of the surface occupied by OC-TRAP staining, suggesting an increase in recruitment and differentiation of OC. Similarly, in HIV-1-Tg rats, a model involving the global transgenic expression of a nonreplicative HIV-1, reduced bone mass was reported, which correlated with a high OC-TRAP staining (18). OC derived from the bone marrow of CD4C-Nef-Tg mice resorbed more and exhibited wider SZ, mimicking the results obtained with human OC infected with HIV-1. Therefore, it is likely that OC participate in the bone remodeling defects evidenced in Nef-Tg mice. Because these mice express Nef in CD4⁺ cells, including T cells, macrophages, OC, and dendritic cells, we propose that the observed bone defects are due, at least in part, to OC expressing Nef in addition to disrupted immune responses, which are known to participate in bone homeostasis (6, 18, 48, 79). Although we do not exclude potential contribution by other viral proteins (80, 81), our results reveal Nef as an essential mediator of the HIV-1 effect on bones (Fig. 9).

It remains to be shown how the virus benefits from manipulating OC. Although OC are giant cells, they do not produce more viral particles than macrophages and these virions exhibit the same infectivity. In contrast with T cells, the cell viability of infected OC is not affected and we can suspect that these infected cells may survive for a long time in bones. Moreover, drug delivery to bones is limited by the unique anatomical features of

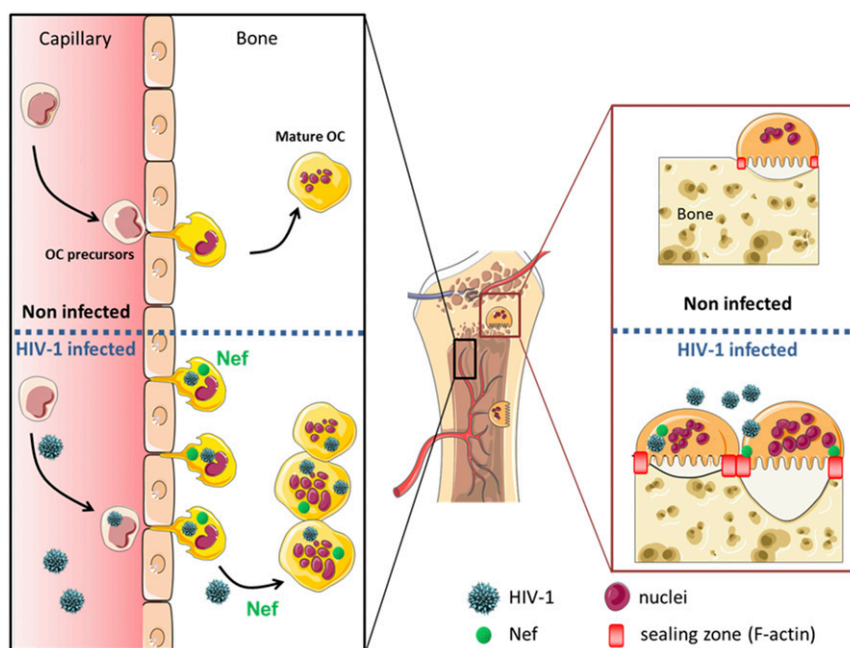


Fig. 9. Graphical abstract proposed to explain HIV-1-induced bone defects in patients. HIV-1 infection affects OC precursor recruitment to bones and the OC differentiation process. These effects, dependent on the viral protein Nef, result in more numerous and more osteolytic OC exhibiting larger and denser SZ.

this tissue (82). Therefore, a putative advantage for the virus may consist in the use of OC as viral reservoirs to hide and survive.

In conclusion, OC are host target cells for HIV-1 that become more osteolytic as a consequence of larger and more degradative SZ. We propose that infected OC participate in bone disorders encountered in HIV-1-infected patients and may constitute a reservoir for the virus. The viral protein Nef appears as a key regulator of the bone resorption activity of OC infected by HIV-1. In summary, this study provides a better understanding of the underlying causes of bone loss following HIV-1 infection.

Materials and Methods

Materials and methods, cell culture and transfection, HIV-1 infection of BLT-humanized mice, viral transfer from infected T cells to primary human OC, cell-free infection of OC and macrophages, and histological analyses of mice bones and of human synovial tissues, are described in *SI Materials and Methods*. Additional materials and methods included flow cytometry analysis, immunoblotting, gel zymography, TRAP staining, IF and transmission electron microscopy analyses, 3D migration, adhesion and resorption assays, chemicals and antibodies, and statistical analysis are also available in *SI Materials and Methods*. Human monocytes were provided by Etablissement Français du Sang, Toulouse, France, under contract 21/PLER/TOU/IPBS01/2013-0042. Experiments with CD4C/HIV Nef mice were approved by the Institutional Animal Ethics committee (Laboratory of Molecular Biology, Clinical Research Institute of Montreal, Montreal, QC, Canada), and experiments with female BLT mice were per-

formed in accordance with guidelines and regulations implemented by the Massachusetts General Hospital Institutional Animal Care and Use Committee.

ACKNOWLEDGMENTS. We thank G. Lugo-Villarino and R. Poincloux for critical reading of the manuscript; C. Salon from US006/Centre Régional d'Exploration Fonctionnelle et de Ressources Expérimentales; M. Dubois, M. Cazabat, M. Requena, and J. Izopet from the BSL3 laboratory of the BiVic facility; F. Moreau and C. Berrone from the animal BSL3 facilities at Institut de Pharmacologie et de Biologie Structurale; C. Bordier for help with cytometry experiments; N. Ortega and A. Métais for help in histology; A. Labrousse for help with RT-PCR; E. Cavaignac for providing synovium samples; E. Meunier for infections with intracellular bacteria; Marie-Chantal Simard and Julio Roberto Caceres-Corte for taking X-rays of Nef-Tg mice, the TRI imaging facility and ANEXPLOR functional exploration facility; Stephanie Balor from the Multiscale Electron Imaging platform of the Centre de Biologie Intégrative for his assistance; and the AIDS Research and Reference Reagent Program, Division of AIDS, National Institute of Allergy and Infectious Diseases. This work was supported by the Centre National de la Recherche Scientifique, the Agence Nationale de la Recherche (ANR 2010-01301, ANR14-CE11-0020-02, ANR16-CE13-0005-01, ANR-11-EQUIPEX-0003); the Agence Nationale de Recherche sur le Sida et les hépatites virales (ANRS2014-CI-2, ANRS2014-049); the Fondation pour la Recherche Médicale (DEQ2016 0334894); INSERM Plan Cancer, the Human Frontier Science Program (RGP0035/2016); German Science Foundation research Fellowship US116-2-1 (to S.M.U.); and National Institutes of Health Grants R01 AI097052 and DA036298 (to T.R.M.). L.B. and S.B. are supported by grants from the Institut Pasteur International Network, Institut Pasteur Shanghai, and the Chinese Academy of Sciences. Work in the P. Jolicœur laboratory was supported by the Canadian Institute of Health Research.

- Cotter AG, Mallon PW (2014) The effects of untreated and treated HIV infection on bone disease. *Curr Opin HIV AIDS* 9:17–26.
- Descours B, et al. (2017) CD32a is a marker of a CD4 T-cell HIV reservoir harbouring replication-competent proviruses. *Nature* 543:564–567, and erratum (2017) 546:686.
- Bruera D, Luna N, David DO, Bergoglio LM, Zamudio J (2003) Decreased bone mineral density in HIV-infected patients is independent of antiretroviral therapy. *AIDS* 17:1917–1923.
- Gibellini D, et al. (2007) RANKL/OPG/TRAIL plasma levels and bone mass loss evaluation in antiretroviral naive HIV-1-positive men. *J Med Virol* 79:1446–1454.
- Grijsen ML, et al. (2010) High prevalence of reduced bone mineral density in primary HIV-1-infected men. *AIDS* 24:2233–2238.
- Titanji K, et al. (2014) Dysregulated B cell expression of RANKL and OPG correlates with loss of bone mineral density in HIV infection. *PLoS Pathog* 10:e1004497.
- Boyle WJ, Simonet WS, Lacey DL (2003) Osteoclast differentiation and activation. *Nature* 423:337–342.
- Prideaux M, et al. (2016) Isolation of osteocytes from human trabecular bone. *Bone* 88:64–72.
- Aziz N, Butch AW, Quint JJ, Detels R (2014) Association of blood biomarkers of bone turnover in HIV-1 infected individuals receiving anti-retroviral therapy (ART). *J AIDS Clin Res* 5:1000360.
- Kotani M, et al. (2013) Systemic circulation and bone recruitment of osteoclast precursors tracked by using fluorescent imaging techniques. *J Immunol* 190:605–612.
- Teitelbaum SL (2011) The osteoclast and its unique cytoskeleton. *Ann N Y Acad Sci* 1240:14–17.
- Georgess D, Machuca-Gayet I, Blangy A, Jurdic P (2014) Podosome organization drives osteoclast-mediated bone resorption. *Cell Adh Migr* 8:191–204.
- Jurdic P, Saltel F, Chabadel A, Destaing O (2006) Podosome and sealing zone: Specificity of the osteoclast model. *Eur J Cell Biol* 85:195–202.
- Luxenburg C, Parsons JT, Addadi L, Geiger B (2006) Involvement of the Src-cortactin pathway in podosome formation and turnover during polarization of cultured osteoclasts. *J Cell Sci* 119:4878–4888.
- Soriano P, Montgomery C, Geske R, Bradley A (1991) Targeted disruption of the c-src proto-oncogene leads to osteopetrosis in mice. *Cell* 64:693–702.

16. Vérollet C, et al. (2013) Hck contributes to bone homeostasis by controlling the recruitment of osteoclast precursors. *FASEB J* 27:3608–3618.
17. Vives V, et al. (2011) The Rac1 exchange factor Dock5 is essential for bone resorption by osteoclasts. *J Bone Miner Res* 26:1099–1110.
18. Vikulina T, et al. (2010) Alterations in the immuno-skeletal interface drive bone destruction in HIV-1 transgenic rats. *Proc Natl Acad Sci USA* 107:13848–13853.
19. de Menezes EG, Machado AA, Barbosa F, Jr, de Paula FJ, Navarro AM (2017) Bone metabolism dysfunction mediated by the increase of proinflammatory cytokines in chronic HIV infection. *J Bone Miner Metab* 35:234–242.
20. Gohda J, et al. (2015) HIV-1 replicates in human osteoclasts and enhances their differentiation in vitro. *Retrovirology* 12:12.
21. Honeycutt JB, et al. (2017) HIV persistence in tissue macrophages of humanized myeloid-only mice during antiretroviral therapy. *Nat Med* 23:638–643.
22. Honeycutt JB, et al. (2016) Macrophages sustain HIV replication in vivo independently of T cells. *J Clin Invest* 126:1353–1366.
23. Sattentau QJ (1988) The role of the CD4 antigen in HIV infection and immune pathogenesis. *AIDS* 2(Suppl 1):S11–S16.
24. Brainard DM, et al. (2009) Induction of robust cellular and humoral virus-specific adaptive immune responses in human immunodeficiency virus-infected humanized BLT mice. *J Virol* 83:7305–7321.
25. Murooka TT, et al. (2012) HIV-infected T cells are migratory vehicles for viral dissemination. *Nature* 490:283–287.
26. Hayder M, et al. (2011) A phosphorus-based dendrimer targets inflammation and osteoclastogenesis in experimental arthritis. *Sci Transl Med* 3:81ra35.
27. Casartelli N, et al. (2010) Tetherin restricts productive HIV-1 cell-to-cell transmission. *PLoS Pathog* 6:e1000955.
28. Iwami S, et al. (2015) Cell-to-cell infection by HIV contributes over half of virus infection. *eLife* 4:e08150.
29. Sewald X, et al. (2015) Retroviruses use CD169-mediated trans-infection of permissive lymphocytes to establish infection. *Science* 350:563–567.
30. Casartelli N (2016) HIV-1 cell-to-cell transmission and antiviral strategies: An overview. *Curr Drug Targets* 17:65–75.
31. Blavier L, Delaissé JM (1995) Matrix metalloproteinases are obligatory for the migration of preosteoclasts to the developing marrow cavity of primitive long bones. *J Cell Sci* 108:3649–3659.
32. Van Goethem E, Poincloux R, Gauffre F, Maridonneau-Parini I, Le Cabec V (2010) Matrix architecture dictates three-dimensional migration modes of human macrophages: Differential involvement of proteases and podosome-like structures. *J Immunol* 184:1049–1061.
33. Vérollet C, et al. (2015) HIV-1 reprograms the migration of macrophages. *Blood* 125:1611–1622.
34. Saltel F, Destaing O, Bard F, Eichert D, Jurdic P (2004) Apatite-mediated actin dynamics in resorbing osteoclasts. *Mol Biol Cell* 15:5231–5241.
35. Väänänen HK, Zhao H, Mulari M, Halleen JM (2000) The cell biology of osteoclast function. *J Cell Sci* 113:377–381.
36. Soe K, Delaissé JM (2017) Time-lapse reveals that osteoclasts can move across the bone surface while resorbing. *J Cell Sci* 130:2026–2035.
37. Geblinger D, Addadi L, Geiger B (2010) Nano-topography sensing by osteoclasts. *J Cell Sci* 123:1503–1510.
38. Destaing O, et al. (2008) The tyrosine kinase activity of c-Src regulates actin dynamics and organization of podosomes in osteoclasts. *Mol Biol Cell* 19:394–404.
39. Moarefi I, et al. (1997) Activation of the Src-family tyrosine kinase Hck by SH3 domain displacement. *Nature* 385:650–653.
40. Saksela K (2011) Interactions of the HIV/SIV pathogenicity factor Nef with SH3 domain-containing host cell proteins. *Curr HIV Res* 9:531–542.
41. Stolp B, Fackler OT (2011) How HIV takes advantage of the cytoskeleton in entry and replication. *Viruses* 3:293–311.
42. Stolp B, et al. (2009) HIV-1 Nef interferes with host cell motility by deregulation of Cofilin. *Cell Host Microbe* 6:174–186.
43. Tribble RP, Emert-Sedlak L, Smithgall TE (2006) HIV-1 Nef selectively activates Src family kinases Hck, Lyn, and c-Src through direct SH3 domain interaction. *J Biol Chem* 281:27029–27038.
44. Noble C, et al. (2010) HIV-1 Nef inhibits ruffles, induces filopodia, and modulates migration of infected lymphocytes. *J Virol* 84:2282–2293.
45. Vérollet C, et al. (2010) HIV-1 Nef triggers macrophage fusion in a p61Hck- and protease-dependent manner. *J Immunol* 184:7030–7039.
46. Mazzolini J, et al. (2010) Inhibition of phagocytosis in HIV-1-infected macrophages relies on Nef-dependent alteration of focal delivery of recycling compartments. *Blood* 115:4226–4236.
47. Swingler S, et al. (2008) Evidence for a pathogenic determinant in HIV-1 Nef involved in B cell dysfunction in HIV/AIDS. *Cell Host Microbe* 4:63–76.
48. Hanna Z, et al. (1998) Nef harbors a major determinant of pathogenicity for an AIDS-like disease induced by HIV-1 in transgenic mice. *Cell* 95:163–175.
49. Hanna Z, et al. (2009) Selective expression of human immunodeficiency virus Nef in specific immune cell populations of transgenic mice is associated with distinct AIDS-like phenotypes. *J Virol* 83:9743–9758.
50. Avalos CR, et al. (2016) Quantitation of productively infected monocytes and macrophages of simian immunodeficiency virus-infected macaques. *J Virol* 90:5643–5656.
51. Cribbs SK, Lennox J, Caliendo AM, Brown LA, Guidot DM (2015) Healthy HIV-1-infected individuals on highly active antiretroviral therapy harbor HIV-1 in their alveolar macrophages. *AIDS Res Hum Retroviruses* 31:64–70.
52. Jambo KC, et al. (2014) Small alveolar macrophages are infected preferentially by HIV and exhibit impaired phagocytic function. *Mucosal Immunol* 7:1116–1126.
53. Smith PD, Meng G, Salazar-Gonzalez JF, Shaw GM (2003) Macrophage HIV-1 infection and the gastrointestinal tract reservoir. *J Leukoc Biol* 74:642–649.
54. Williams KC, et al. (2001) Perivascular macrophages are the primary cell type productively infected by simian immunodeficiency virus in the brains of macaques: Implications for the neuropathogenesis of AIDS. *J Exp Med* 193:905–915.
55. Benaroch P, Billard E, Gaudin R, Schindler M, Jouve M (2010) HIV-1 assembly in macrophages. *Retrovirology* 7:29.
56. Tan J, Sattentau QJ (2013) The HIV-1-containing macrophage compartment: A perfect cellular niche? *Trends Microbiol* 21:405–412.
57. Welsch S, et al. (2007) HIV-1 buds predominantly at the plasma membrane of primary human macrophages. *PLoS Pathog* 3:e36.
58. Sattentau QJ, Stevenson M (2016) Macrophages and HIV-1: An unhealthy constellation. *Cell Host Microbe* 19:304–310.
59. Delobel P, et al. (2005) Persistence of distinct HIV-1 populations in blood monocytes and naive and memory CD4 T cells during prolonged suppressive HAART. *AIDS* 19:1739–1750.
60. Zhu T, et al. (2002) Evidence for human immunodeficiency virus type 1 replication in vivo in CD14(+) monocytes and its potential role as a source of virus in patients on highly active antiretroviral therapy. *J Virol* 76:707–716.
61. Bracq L, et al. (2017) T cell-macrophage fusion triggers multinucleated giant cell formation for HIV-1 spreading. *J Virol* 91:e01237-17.
62. Law KM, et al. (2016) In vivo HIV-1 cell-to-cell transmission promotes multicopy micro-compartmentalized infection. *Cell Rep* 15:2771–2783.
63. Russell RA, Martin N, Mitar I, Jones E, Sattentau QJ (2013) Multiple proviral integration events after virological synapse-mediated HIV-1 spread. *Virology* 443:143–149.
64. Sigal A, et al. (2011) Cell-to-cell spread of HIV permits ongoing replication despite antiretroviral therapy. *Nature* 477:95–98.
65. Baxter AE, et al. (2014) Macrophage infection via selective capture of HIV-1-infected CD4+ T cells. *Cell Host Microbe* 16:711–721.
66. Dale BM, Alvarez RA, Chen BK (2013) Mechanisms of enhanced HIV spread through T-cell virological synapses. *Immunol Rev* 251:113–124.
67. Eugenin EA, Gaskill PJ, Berman JW (2009) Tunneling nanotubes (TNT) are induced by HIV-infection of macrophages: A potential mechanism for intercellular HIV trafficking. *Cell Immunol* 254:142–148.
68. Sattentau Q (2008) Avoiding the void: Cell-to-cell spread of human viruses. *Nat Rev Microbiol* 6:815–826.
69. Sowinski S, et al. (2008) Membrane nanotubes physically connect T cells over long distances presenting a novel route for HIV-1 transmission. *Nat Cell Biol* 10:211–219.
70. Wiesner C, Le-Cabec V, El Azzouzi K, Maridonneau-Parini I, Linder S (2014) Podosomes in space: Macrophage migration and matrix degradation in 2D and 3D settings. *Cell Adh Migr* 8:179–191.
71. Proag A, et al. (2015) Working together: Spatial synchrony in the force and actin dynamics of podosome first neighbors. *ACS Nano* 9:3800–3813.
72. Stenbeck G, Horton MA (2000) A new specialized cell-matrix interaction in actively resorbing osteoclasts. *J Cell Sci* 113:1577–1587.
73. Merriild DM, et al. (2015) Pit- and trench-forming osteoclasts: A distinction that matters. *Bone Res* 3:15032.
74. Panwar P, et al. (2016) A novel approach to inhibit bone resorption: Exosite inhibitors against cathepsin K. *Br J Pharmacol* 173:396–410.
75. Vives V, et al. (2015) Pharmacological inhibition of Dock5 prevents osteolysis by affecting osteoclast podosome organization while preserving bone formation. *Nat Commun* 6:6218.
76. Foster JL, Garcia JV (2006) HIV pathogenesis: Nef loses control. *Cell* 125:1034–1035.
77. Stolp B, et al. (2012) HIV-1 Nef interferes with T-lymphocyte circulation through confined environments in vivo. *Proc Natl Acad Sci USA* 109:18541–18546.
78. Vérollet C, Le Cabec V, Maridonneau-Parini I (2015) HIV-1 infection of T lymphocytes and macrophages affects their migration via Nef. *Front Immunol* 6:514.
79. Hanna Z, et al. (2001) The pathogenicity of human immunodeficiency virus (HIV) type 1 Nef in CD4C/HIV transgenic mice is abolished by mutation of its SH3-binding domain, and disease development is delayed in the absence of Hck. *J Virol* 75:9378–9392.
80. Chew N, Tan E, Li L, Lim R (2014) HIV-1 tat and rev upregulates osteoclast bone resorption. *J Int AIDS Soc* 17(Suppl 3):19724.
81. Gibellini D, et al. (2010) HIV-1 Tat protein enhances RANKL/M-CSF-mediated osteoclast differentiation. *Biochem Biophys Res Commun* 401:429–434.
82. Hirabayashi H, Fujisaki J (2003) Bone-specific drug delivery systems: Approaches via chemical modification of bone-seeking agents. *Clin Pharmacokinet* 42:1319–1330.